

Effects of metallic electrodes on the thermoelectric properties of quantum dot array realized by zigzag graphene nanoribbons with periodic vacancies

David M T Kuo

*Department of Electrical Engineering and Department of Physics,
National Central University, Chungli, 320 Taiwan*

(Dated: December 6, 2022)

In this work, we theoretically study the thermoelectric properties of a graphene quantum dot array (GQDA) with line and surface contacted metal electrodes. Such GQDAs are realized by zigzag graphene nanoribbons (ZGNRs) with periodic vacancies. The gaps and minibands are formed in these GQDAs, which could have metallic and semiconducting phases. The electronic states of first conduction (valence) miniband with nonlinear dispersion could remain very long coherent lengths along the zigzag edge direction. In the line contacted metal electrodes, the GQDAs show the characteristic of serially coupled QDs (SCQDs) when the armchair edge atoms of ZGNRs are coupled to the electrodes. On the other hand, the GQDAs show the characteristic of parallel QDs when the zigzag edge atoms are coupled to the electrodes. The maximum thermoelectric power factors of SCQDs with different line contacted electrodes such as *Cu*, *Au*, *Pt*, *Pd* and *Ti* at room temperature are very close and beyond $0.186nW/K$, while their figure of merits are larger than three. The thermoelectric performance of a GQDA with line contacted metal electrodes is much better than that with surface contacted metal electrodes.

I. INTRODUCTION

The semiconductor quantum dot (QD) nanostructures exhibit atom-like discrete electron energy levels. High efficiency nanostructure devices show the functionalities of low electrical and optical power outputs. These low power devices include single electron transistors[1-3], single photon sources[4-6], single photon detectors[7] and single electron heat engines[8]. Some applications of QD devices require both high efficiency and significant output power. Therefore, one needs QD solids that can retain the size tunable properties of the QDs while exhibiting the band transport characteristic of bulk semiconductors.[9] Although much effort has been devoted to producing such QD solids, experimental studies of the thermoelectric properties of such 1D QD arrays have been lacking.[10,11] The thermoelectric devices made of 1D silicon quantum dot arrays (QDAs) exist the dot-size fluctuation issue.[12]

Recently, extensive studies have focused on two-dimensional materials such as graphenes,[13] and 2D transition metal dichalcogenides (TMDs) and oxides [14-16]. Now one can fabricate quasi-1D graphene nanoribbons (GNRs) with atomic precision via the bottom-up approach[17], this approach is able to build more complex graphene-based nanostructures on-demands for quantum device applications [18-28]. The superlattices of zigzag GNRs (ZGNRs) behave as graphene quantum dot arrays (GQDAs) .[29] The phonon thermal conductance of GQDAs can be dramatically reduced at least one order magnitude than that of ZGNRs.[30]. Therefore, it is expected that GQDAs have promising applications in nanoscale energy harvesting.

Nevertheless, previous studies have demonstrated that the contact types of graphene and GNRs are significantly to influence electron transport between the electrodes.[31-33] To reduce electron backward scatter-

ing components, the transmission coefficient of GNRs prefer the normal metal electrodes rather than graphene electrodes.[32] In addition, the contact resistance of a graphene with line contacted metal electrodes can be much smaller than that of a graphene with surface contacted metal electrodes.[33] Other 2D materials also remain such a feature.[34,35] All these results indicate that interface property arising from contact junction is a critical issue to implement graphene-based or TMD-based electronic and thermoelectric devices.

So far not many studies have examined the effects of the various contacted metal materials and geometries on the performance of GQDA thermoelectric devices. In this study, we theoretically investigate the ballistic transport and thermoelectric properties of GQDAs coupled to the different metal electrodes as shown in Fig. 1, where GQDAs are realized by ZGNRs with periodic vacancies. We have focused on the channel length between thermal contact shorter than electron mean free path (λ_e), but longer than phonon mean free path (λ_{ph}). We have calculated electrical conductance (G_e), Seebeck coefficient (S) and electron thermal conductance (κ_e) for different line contacted metal electrodes and surface contacted metal electrodes in the framework of tight binding model and Green's function approach. We find that the maximum thermoelectric power factor values of GQDAs with different *Cu*, *Au*, *Pt*, *Pd* and *Ti* line contacted electrodes can have 79% of power factor of 1D theoretical limit at room temperature.

II. CALCULATION METHOD

It is a good approximation to employ a tight-binding model with one p_z orbital per atomic site to describe the electronic states of a GQDA realized by ZGNRs with periodic vacancies.[29,36] The Hamiltonian of the GQDA

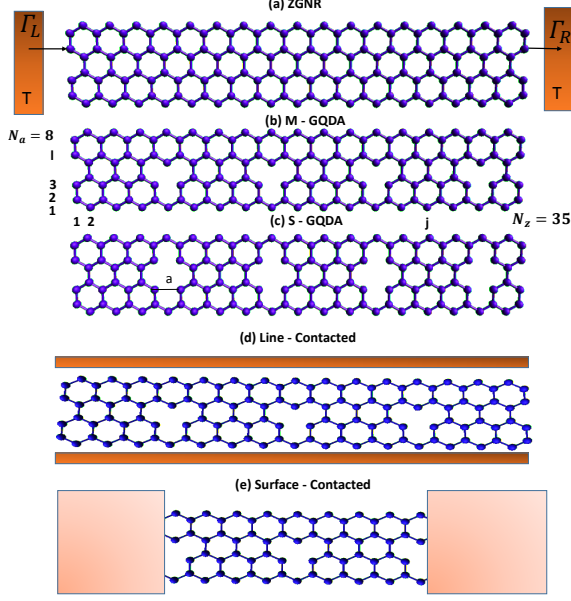


FIG. 1: Schematic diagram of a zigzag graphene nanoribbon (ZGNR) without and with vacancies for $N_a = 8$ and $N_z = 35$. (a) Armchair edge atoms of ZGNRs are coupled to metallic electrodes. Γ_L (Γ_R) denotes the tunneling rate of the electrons between the left (right) electrode and the leftmost (rightmost) carbon atoms of the armchair edges. T denotes the equilibrium temperature of the left (right) electrode. (b,c) Graphene quantum dot arrays (GQDAs) are realized by periodically removing one carbon and two carbons of interior sites of ZGNRs. The distance between the nearest vacancies is $D = 4a$, where the lattice constant of graphene is $a = 2.46\text{\AA}$. (d) The zigzag edge atoms of GQDAs are coupled to the metal electrodes. (e) GQDAs have the surface contacted metal electrodes.

can be written as H_{GQDA} where

$$H_{GQDA} = \sum_{\ell,j} E_{\ell,j} d_{\ell,j}^\dagger d_{\ell,j} - \sum_{\ell,j} \sum_{\ell',j'} t_{(\ell,j),(\ell',j')} d_{\ell,j}^\dagger d_{\ell',j'} + h.c., \quad (1)$$

where $E_{\ell,j}$ is the on-site energy for the p_z orbital in the ℓ -th row and j -th column. $d_{\ell,j}^\dagger$ ($d_{\ell,j}$) creates (destroys) one electron at the atom site labeled by (ℓ,j) where ℓ and j , respectively are the row and column indices as illustrated in Fig. 1. $t_{(\ell,j),(\ell',j')}$ describes the electron hopping energy from site (ℓ,j) to site (ℓ',j') . The tight-binding parameters used for GQDAs are $E_{\ell,j} = 0$ for the on-site energy and $t_{(\ell,j),(\ell',j')} = t_{pp\pi} = 2.7\text{ eV}$ for the nearest-neighbor hopping strength. Here, the electron electron Coulomb interactions are neglected. Their effect will be discussed in later.

Thermoelectric coefficients including electrical conductance (G_e), Seebeck coefficient (S) and electron ther-

mal conductance (κ_e) are calculated by $G_e = e^2 \mathcal{L}_0$, $S = -\mathcal{L}_1/(eT\mathcal{L}_0)$ and $\kappa_e = \frac{1}{T}(\mathcal{L}_2 - \mathcal{L}_1^2/\mathcal{L}_0)$ with \mathcal{L}_n ($n = 0, 1, 2$) defined as

$$\mathcal{L}_n = \frac{2}{h} \int d\varepsilon \mathcal{T}_{LR}(\varepsilon) (\varepsilon - \mu)^n \frac{\partial f(\varepsilon)}{\partial \mu}. \quad (2)$$

Here $f(\varepsilon) = 1/(\exp^{(\varepsilon - \mu)/k_B T} + 1)$ is the Fermi distribution function of electrodes at equilibrium temperature T and chemical potential μ . $\mathcal{T}_{LR}(\varepsilon)$ denotes the transmission coefficient of a GQDA connected to electrodes, which can be solved by the formula $\mathcal{T}_{LR}(\varepsilon) = 4Tr[\Gamma_L(\varepsilon)G^r(\varepsilon)\Gamma_R(\varepsilon)G^a(\varepsilon)]$ [37-39], where $\Gamma_L(\varepsilon)$ and $\Gamma_R(\varepsilon)$ denote the tunneling rate at the left and right leads, and $G^r(\varepsilon)$ and $G^a(\varepsilon)$ are the retarded and advanced Green's function of the GQDA. The tunneling rates are described by the imaginary part of self energy resulting from the coupling between the left (right) electrode with its adjacent atoms of GQDAs. In the basis of tight-binding orbitals $\Gamma_\alpha(\varepsilon)$ and Green's functions are matrices. For simplicity, Γ_α for interface carbon atoms have diagonal entries given by the same constant Γ_t . The magnitudes of Γ_t depend on the line contacted metal electrodes or surface contacted metal electrodes.[33]

III. RESULTS AND DISCUSSION

A. Electronic energy levels

A graphene with a semi-metallic phase limits its device applications[40,41]. Nevertheless, a graphene with periodic vacancies exhibits minibands, which open the door for graphene in the applications of thermoelectric devices at low temperatures.[42,43] To realize a graphene-based devices operating at room temperature, some studies have considered ZGNRs with periodic vacancies [44] However, there is a paucity of studies to investigate how the line and surface contacted metal electrodes influence the thermoelectric properties of ZGNRs with vacancies. Before discussing the effect of contact, we illustrate the electron band structures of ZGNRs without and with periodic vacancies in Fig. 2. The band structures of ZGNRs with various widths (N_a) have been extensively studied. [40] The localized zero energy flat-band modes of the first subband are from $k = \frac{2\pi}{3a}$ to $\frac{\pi}{a}$ as $N_a \rightarrow \infty$. In Fig. 2(a), the states of the first subband are the localized states for k within $k_c = 0.738\frac{\pi}{a} \leq k \leq \frac{\pi}{a}$, where k_c is determined by $k_c/2 = \arccos(N_a/(2N_a + 4))$ and $N_a = 8$. [36] The edge state with a shortest decay length along the armchair direction occurs at $k = \frac{\pi}{a}$. When k is deviating from $\frac{\pi}{a}$, the zigzag edges states form the bonding and antibonding states. Therefore, the zero-energy modes are lifted in Fig. 2(a). When $|E| \geq 2.16\text{ eV}$, we observe the second conduction and valence subbands. Because they are bulk states, this study has focused on the edge states of first subband with $|E| \leq 2.16\text{ eV}$. For ZGNRs with periodic vacancies, as seen in Fig. 2(b) and Fig. 2(c),

the gapped energy regions are opened and minibands are formed. The ZGNR with periodic vacancies can be in the semiconducting phase as illustrated by the sizable central gap (0.959 eV) in Fig. 2(c). To distinguish their phase difference, from now on we call them, respectively, as metal GQDA (M-GQDA) and semiconductor GQDA (S-GQDA). Because of a finite channel length short than λ_e and larger than λ_{ph} , the length-dependent energy levels of GQDAs should be further clarified.

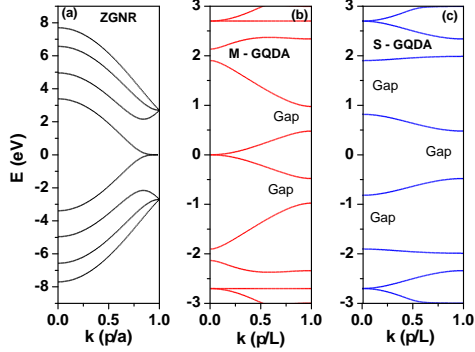


FIG. 2: Electronic band structures of ZGNRs without and with periodic vacancies. The distance between the nearest vacancies is $L = 4a$, which is considered throughout this article. The size of a super unit cell is characterized by $N_a = 8$ and $N_z = 8$.

To illustrate the characteristic of energy levels in each miniband shown in Fig. 2(b) and 2(c), we show the calculated eigenvalues as functions of QD number N_{QD} (or $N_z = 8N_{QD} - 1$) in Fig. 3. The spectra show the transformation from the molecule-like to the band-like situation when N_{QD} increases from 3 to a infinity (see Fig. 2). As seen in Fig. 3, the number of energy levels in each miniband is given by N_{QD} . This demonstrates that ZGNRs with periodic vacancies show the manifested characteristic of GQDAs. A single GQD can be characterized by size of $N_a = 8$ and $N_z = 7$ which gives the four energy levels of $\varepsilon_{h,2} = -1.9024$ eV, $\varepsilon_{h,1} = -0.47905$ eV, $\varepsilon_{e,1} = 0.47905$ eV and $\varepsilon_{e,2} = 1.9024$ eV in the range of $|E| \leq 2.16$ eV. These four energy levels are insensitive to the increase of N_{QD} . In order to understand such a behavior, we calculate the eigenvalues of ZGNRs without periodic vacancies as a function of $N_z = 8N_{QD} - 1$ for $N_a = 8$ and find the result of N_z -independent $\varepsilon_{e(h),1}$ and $\varepsilon_{e(h),2}$. This indicates that such a behavior does not arise from periodic vacancies. The wave functions of $\varepsilon_{e(h),1}$ and $\varepsilon_{e(h),2}$ of the ZGNRs are vanishingly small at $j = 8m$ (so called nodes), where m is an integer. That explains the behavior of N_{QD} -independent $\varepsilon_{e(h),1}$ and $\varepsilon_{e(h),2}$ in Fig. 3. The sinusoidal wave of $\varepsilon_{e(h),1}$ ($\varepsilon_{e(h),2}$) along the zigzag edges gives a very longer coherence length. Although the periodic vacancies do not affect the energy levels of $\varepsilon_{e(h),1}$ and $\varepsilon_{e(h),2}$, they restrict and perturb some energy levels of ZGNRs. Therefore, they have the name of

antidots.[42-44]

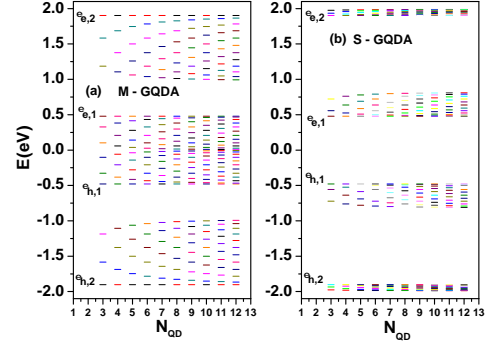


FIG. 3: (a) Spectra of M-GQDA as functions of N_{QD} and (b) spectra of S-GQDA as functions of N_{QD} . Each GQD in the GQDA structures has size $N_a = 8$ and $N_z = 7$. The length of GQDA is given by $N_z = 8N_{QD} - 1$.

B. Line contacted metal electrodes

When a graphene is coupled to metal electrodes, contact properties such as the Schottky barrier or ohmic contact and contact geometries can significantly influence electron transport in graphene.[33,45-56] Even though many theoretical studies tried to clarify this critical issue by using the first principle method, one can obtain only qualitative results of Γ_t arising from contact junction due to the limitation of theory.[57,58] In Fig. 4 we show the calculated transmission coefficient of interface $T_c(\varepsilon)$ based on the configuration considered in ref.[33] where authors introduced the super unit cells with eight unit cells and considered the armchair edge atoms of graphene coupled to different metal electrodes. Contact resistance $R_c = 1/G_{e,c}$ per unit cell is determined by $G_{e,c} = G_0 T_c(\varepsilon = 0)$, where $G_0 = 2e^2/h = 1/(12.9k\Omega) = 77.5\mu S$ is the quantum conductance and $T_c(\varepsilon = 0)$ is the contact transmission coefficient at the Fermi energy. In ref[33], authors gave $R_c = 13.3, 17.8, 18.6, 23.3$ and $31.7 k\Omega$ for Ti, Pd, Pt, Au and Cu , respectively. The Γ_t of each carbon atom at the interface can be obtained by fitting these contact resistances. We obtain the Γ_t values of Cu, Au, Pt, Pd , and Ti as $\Gamma_t = 0.495$ eV, $\Gamma_t = 0.603$ eV, $\Gamma_t = 0.693$ eV, $\Gamma_t = 0.72$ eV, and $\Gamma_t = 0.9$ eV, respectively.

1. Armchair edge atoms coupled to electrodes

Based on above Γ_t values, we show in Fig. 5 the calculated $\mathcal{T}_{LR}(\varepsilon)$ of M-GQDA with $N_a = 8$ and $N_z = 127$ for various metal electrodes. The maximum $\mathcal{T}_{LR}(\varepsilon) = 1$ indicates that GQDAs behave as a serially coupled QDs (SCQD). Note that two energy levels $\varepsilon_{e(h)} = \pm 0.47905$ eV

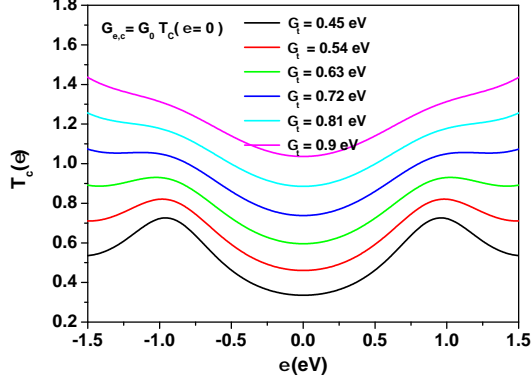


FIG. 4: Transmission coefficient at the metal-graphene interface per unit cell for various Γ_t values. Armchair edge atoms of graphene are coupled to metal electrodes. Super unit cell includes 16 carbon atoms.

and $\varepsilon_{e(h)} = \pm 0.47179 \text{ eV}$ are too close to be resolved in the spectra of $\mathcal{T}_{LR}(\varepsilon)$. From Eq. (2), the area below $\mathcal{T}_{LR}(\varepsilon)$ curve plays a considerable role on the thermoelectric coefficients. As seen in Fig. 5, the area below the $\mathcal{T}_{LR}(\varepsilon)$ curve is enhanced with increasing tunneling rate. Meanwhile, these areas remain a near right triangle shape that has a steep change with respect to ε on the sides of $\varepsilon_{e,1}$ and $\varepsilon_{h,1}$ edges. For energy harvesting applications at room temperature, we need to design a $\mathcal{T}_{LR}(\varepsilon)$ spectrum with a square form (SF) to obtain optimized figure of merit and electrical power output.[59] Up to now it remains unclear how to realize the area of $\mathcal{T}_{LR}(\varepsilon)$ curve with SF in a finite channel length ($L_z < \lambda_e$) between thermal contacts.[39]

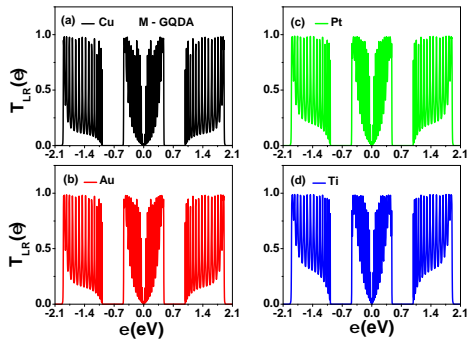


FIG. 5: Transmission coefficient $\mathcal{T}_{LR}(\varepsilon)$ of a finite M-GQDA as functions of ε for different line contacted metal electrodes at $N_a = 8$ ($L_a = 0.71 \text{ nm}$) and $N_z = 127$ ($L_z = 15.5 \text{ nm}$). Diagrams (a), (b), (c) and (d) correspond to *Cu*, *Au*, *Pt* and *Ti*, respectively.

Next, we calculate electrical conductance (G_e), Seebeck coefficient (S), power factor (PF) and figure of merit (ZT) of M-GQDAs at room temperature in Fig.

6. G_e , S and PF are in units of $G_0 = 2e^2/h$, $k_B/e = 86.25 \mu\text{V/K}$ and $2k_B^2/h = 0.575 \text{ pW/K}^2$, respectively. Unlike G_e , S is less sensitive to the variation of Γ_t as indicated in Fig. 6b. The behavior of S can be roughly illustrated by $S = -\frac{\pi^2 k_B^2 T}{3e} \frac{\partial \ln(G_e(\mu, T))}{\partial \mu}$. The maximum PF and ZT values are given by μ in the gap region. The trend of ZT with respect to various metal electrodes is determined by the power factor ($PF = S^2 G_e$) since the thermal conductance of GQDAs is dominated by phonon thermal conductance κ_{ph} . We calculated dimensionless $ZT = S^2 G_e T / (\kappa_e + \kappa_{ph})$ with $\kappa_{ph} = F_s \kappa_{ph, ZGNR}$ where $\kappa_{ph, ZGNR} = \frac{\pi^2 k_B^2 T}{3h}$ is the phonon thermal conductance of an ideal ZGNR [60] and $F_s = 0.1$ denotes a reduction factor resulting from periodic vacancies in ZGNRs.[30,43]. The results shown in Fig. 6 implies that $ZT > 3$ could be realized by considering GQDAs coupled to metallic electrodes. These four different metal electrodes have very closer maximum PF and ZT values. The maximum PF can reach 79% of the theoretical limit of 1D systems with $PF_{QB} = 1.2659 (\frac{2k_B^2}{h})$. [59] Note that ZGNRs are graphene-based 1D topological insulators (TIs). ZT of 1D TIs larger 3 has been theoretically demonstrated in the absence of periodic vacancies. [61] The maximum ZT values of 1D TIs prefer the position of μ near the minimum value of second subband shown in Fig. 2(a) ($|E| = 2.16 \text{ eV}$).

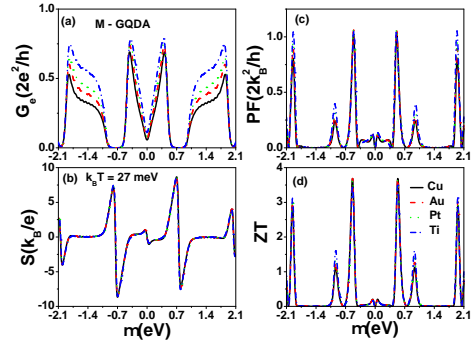


FIG. 6: (a) Electrical conductance G_e , (b) Seebeck coefficient S , (c) power factor ($PF = S^2 G_e$) and (d) figure of merit ZT as functions of μ for various metal electrodes at $k_B T = 27 \text{ meV}$.

In Fig. 6(b), the gaps between the minibands are significantly to enhance the maximum S values. Therefore, it is interesting to investigate the thermoelectric properties of S-GQDAs with a large central band gap. We show the calculated transmission coefficient of S-GQDAs for various line contacted metal electrodes in Fig. 7. Compared with the miniband widths of M-GQDAs, S-GQDAs have much smaller miniband widths, which highly reduce the area of $\mathcal{T}_{LR}(\varepsilon)$ curves. In Fig. 8, we show the calculated G_e , S , power factor $PF = S^2 G_e$ and ZT as functions of μ at room temperature. Due to the electron-hole symmetry, we have considered the range of chemi-

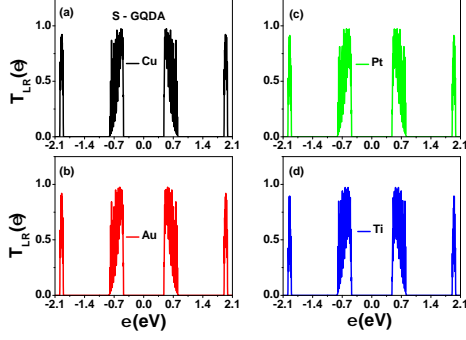


FIG. 7: Transmission coefficient $\mathcal{T}_{LR}(\varepsilon)$ of a finite S-GQDA as functions of ε for different line contacted metal electrodes at $N_a = 8$ ($L_a = 0.71\text{nm}$) and $N_z = 127$ ($L_z = 15.5\text{nm}$). Diagrams (a), (b), (c) and (d) correspond to *Cu*, *Au*, *Pt* and *Ti*, respectively.

cal potential $\mu \geq 0$. The G_e spectra of the first miniband remain the triangular shape characteristic like Fig. 6(a), but the steep change with respect to μ is toward the central gap. Because of large gaps, the maximum Seebeck coefficients in Fig. 8(b) are almost two times larger than those of Fig. 6(b). The maximum power factor $PF_{max}(\mu = 0.45\text{eV}) = 0.9682$ and figure of merit $ZT_{max}(\mu = 0.427\text{eV}) = 3.442$ occur at the chemical potentials near the $\varepsilon_{e,1} = 0.47905\text{eV}$ for *Cu* electrodes. The considered κ_{ph} value is the same as that of Fig. 6(d). Comparison between the maximum ZT of Fig. 8(d) and that of Fig. 6(d), we found that the maximum ZT value does not increase although the maximum S is highly enhanced. In the situation of $\kappa_{ph} \gg \kappa_e$, the enhancement of G_e is also important. When the miniband width become small, the G_e is suppressed in the gap region. In Fig. 8(c) and 8(d), $PF_{max,2}$ and $ZT_{max,2}$ are also smaller than $PF_{max,1}$ and $ZT_{max,1}$. Such results indicate that the enhancement of electrical power output needs not only large gaps but also wider miniband widths.

2. Zigzag edge atoms coupled to electrodes

Our previous study has demonstrated that the electron transport of finite ZGNRs significantly depend on armchair or zigzag edge sides coupled to electrodes.[38] According to the works of ref[58], most of edge-oxidized modifications will dramatically change the electron band structures of ZGNRs. Therefore, we avoid the case of edge-oxidized GNRs in the following discussions. The contact resistance of Cr/X/graphene has been calculated in refs[48], where the zigzag edge atoms of graphene are coupled to *Cr* via the bridge of different atoms (*H*, *F*, *O* and *S*). Due to a large binding distance, the very high contact resistance is observed in the Cr/H/graphene structure. We adopt, respectively, $\Gamma_t = 9\text{ meV}$ and $\Gamma_t = 45\text{ meV}$ for Cr/H/GQDAs and Cr/F/GQDAs, to

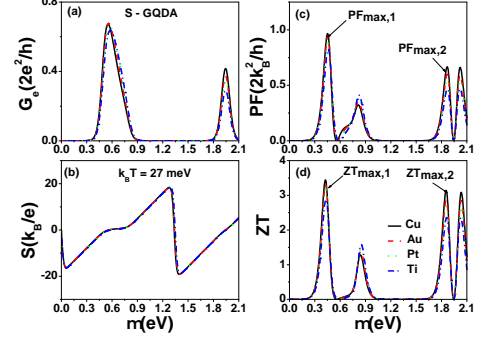


FIG. 8: (a) Electrical conductance G_e , (b) Seebeck coefficient S , (c) power factor $PF = S^2 G_e$ and (d) figure of merit (ZT) of S-GQDSLs as functions of μ for various metal electrodes at $k_B T = 27\text{meV}$.

calculate G_e as functions of μ at zero temperature in Fig.9, where M-GQDAs and S-GQDAs have $N_a = 8$ and $N_z = 127$. As seen in Fig. 9, the spectra of G_e are larger than quantum conductance $G_0 = \frac{2e^2}{h}$. It demonstrates that GQDAs behave as parallel QDs when the zigzag edge atoms of M-GQDAs and S-GQDAs are coupled to the metal electrodes. In parallel QD configuration the spectra resulting from the electronic states near the zero energy modes of M-GQDAs and the high energy modes of the first minibands of S-GQDAs can be very significant if compared to the spectra of Fig. 5 and Fig. 7.

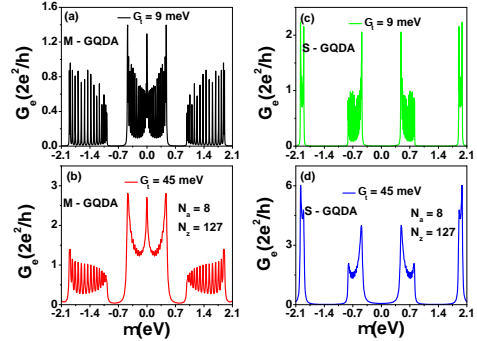


FIG. 9: Electrical conductance as functions of μ for $\Gamma_t = 9\text{ meV}$ and $\Gamma_t = 45\text{ meV}$. (a) and (b) consider M-GQDAs, and (c) and (d) consider S-GQDAs. Their sizes are $N_a = 8$ ($L_a = 0.71\text{ nm}$) and $N_z = 127$ ($L_z = 15.5\text{ nm}$).

Fig. 10 shows the calculated S and PF of M-GQDAs and S-GQDAs at room temperature ($k_B T = 27\text{ meV}$). The maximum S is degraded very seriously for a parallel QD configuration with a short channel length of $L_a = 0.71\text{ nm}$ if compared with the maximum S values of Fig. 6 and Fig. 8. This is attributed to the highly enhanced G_e in a gap region, which is similar to the metal induced gap states in metal-semiconductor Schot-

tky junctions.[62] When the zigzag edge atoms are coupled to the metal electrodes, the miniband edge states are readily extended into the gap regions for a short channel length. Although, the maximum PF as seen in Fig. 10 is much larger than $PF_{QB} = 1.2659(\frac{2k_B^2}{h})$, their ZT values are smaller than one due to the remarkable enhancement of electron thermal conductance (κ_e) and phonon thermal conductance (κ_{ph}).

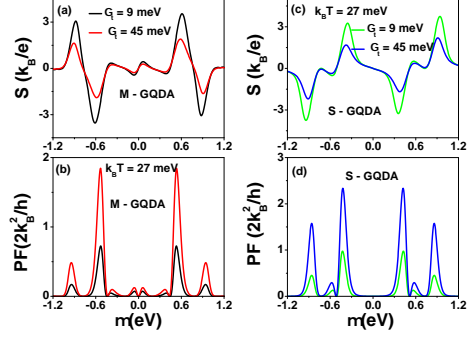


FIG. 10: (a) Seebeck coefficient and (b) power factor of M-GQDAs as functions of μ for two different tunneling rates at $k_B T = 27\text{meV}$. (c) Seebeck coefficient and (d) power factor of S-GQDAs as functions of μ for different tunneling rates at $k_B T = 27\text{meV}$. Other physical parameters are the same as those of Fig. 9.

C. Surface contacted metal electrodes

So far few experimental studies have reported the transport and thermoelectric properties of GNRs due to the difficulty of line contacted technique.[63] From experimental point of view, it is relatively easy to lay out surface contacted metal electrodes. Therefore, it is desirable to reveal thermoelectric properties of GNRs with surface contacted electrodes. Many theoretical literatures have demonstrated that surface contact resistance is ten to thousand times larger than line contact resistance.[33,45-56] This indicates that Γ_t could be a very small value. We show the calculated transmission coefficient of M-GQDA as functions of μ for various Γ_t values in Fig. 11, where the two outer GQDs coupled to metallic electrodes. There are 28 carbon atoms including 6 carbon atoms located at zigzag edge sites under surface contacted left (right) metal electrode. Due to small Γ_t values, the peaks of $\mathcal{T}_{LR}(\varepsilon)$ spectra are very narrow. The molecule-like spectra will degrade the electrical conductance at room temperature.

In Fig. 12 we show the calculated G_e , κ_e , PF and ZT as functions of μ for different temperatures at surface contacted metal electrodes. In comparison with electrical conductance of Fig.6(a) the maximum $G_e = 0.25G_0$ at room temperature is much smaller. Unlike the behav-

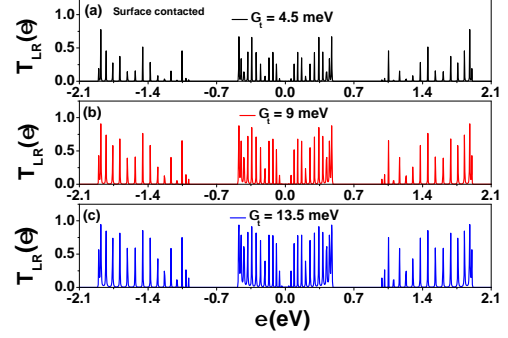


FIG. 11: Transmission coefficient of a M-GQDA with $N_a = 8$ and $N_z = 127$ as functions of ε for various Γ_t values. (a), (b) and (c) correspond to $\Gamma_t = 4.5$ meV, 9 meV and 13.5 meV, respectively. Surface contacted metal electrodes are considered.

ior of G_e with respect to temperature, electron thermal conductance κ_e is enhanced with increasing temperature. Here, κ_e is in units of $\kappa_0 = 0.62nW/K$. The enhancement of maximum PF with decreasing temperature is attributed to the enhancement of S , which is a very non-linear function of temperature. In the calculation of ZT , κ_{ph} is the same as that of Fig. 5. At room temperature, the maximum value of $ZT(\mu = 0.535\text{eV}) = 1.9927$ is smaller than three. However, the maximum PF and ZT values are enhanced with decreasing temperature. When the spectra of G_e show a molecule-like characteristic, the thermoelectric performance of GQDAs remains useful in the low temperature region.[64]

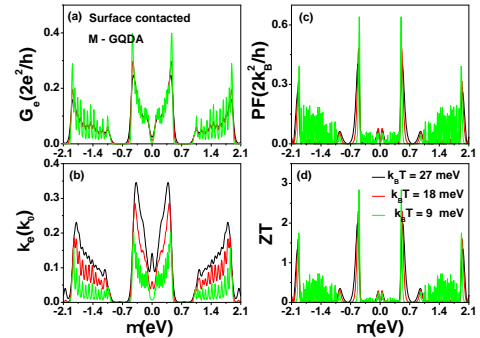


FIG. 12: (a) Electrical conductance, (b) electron thermal conductance, (c) power factor and (d) figure of merit as functions of μ for various temperatures for M-GQDA with surface contacted metal electrodes. We have adopted $\Gamma_t = 14.5$ meV. Other physical parameters are the same as those of Fig. 11.

We find that the molecule-like or band-like spectra of GQDAs are determined not only the lengths of GQDAs but also contact geometry. In the line contacted metal electrodes, the spectra of finite GQDAs function as a

band-like characteristic due to large Γ_t values. On the other hand, the spectra of finite GQDAs have a molecule-like characteristic for the surface contacted metal electrodes. So far, we have not investigated the effect of electron-electron Coulomb interactions in this study. Although electron Coulomb interactions are strong in small GQDAs ($L_a = 0.71$ nm and $L_z = 15.5$ nm), their effects on the thermoelectric quantities can be neglected when electron transports are dominated by the thermionic-assisted tunneling procedure (TATP), which occurs at μ away from the minibands. Thermionic electron population in the minibands is very dilute when μ locates inside the gap. As a result, electron correlation functions arising from electron Coulomb interactions are small[64-66]. The calculated maximum PF and ZT are valid in the TATP.

IV. CONCLUSION

Although ZGNRs show the metallic phases, the minibands and the gaps are formed for the ZGNRs with periodic vacancies, which behave as GQDAs. Such GQDAs can host metallic and semiconductor phases. The edge states of first conductance and valence minibands such as $\varepsilon_{e(h),1}$ are localized edge states along armchair edge direction, whereas they have very long coherent lengths along zigzag edge direction. The designed GQDAs have large enough gaps and miniband widths, therefore, they

are valuable to implement thermoelectric devices operating at room temperature. In the line contacted metal electrodes, the maximum power factor (figure of merit) of the M-GQDAs at room temperature is larger than that of the S-GQDAs due to the M-GQDAs with wider miniband widths. The GQDAs behave as a serially coupled QDs (SCQDs) when the armchair edge atoms are coupled to the metal electrodes. On the other hand, The GQDAs behave as a parallel coupled QDs when zigzag edge atoms are coupled to metal electrodes. In the situation of SCQDs with line contacted electrodes, the maximum power factor values of GQDAs with different metal electrodes (*Cu*, *Au*, *Pt*, *Pd* and *Ti*) at room temperature can reach 79% of the theoretical limit of 1D systems, while their figure of merits are larger than three. For the surface contacted metal electrodes, the spectra of electrical conductance of the finite M-GQDAs show the molecule-like spectra characteristic because of high contact surface resistance. The thermoelectric power factor and figure of merit of the M-GQDAs at room temperature are smaller than those in the line contacted situations, however their ZT values at low temperatures can reach three.

Acknowledgments

We thank Yia-Chung Chang for valuable discussions.

-
- ¹ L. J. Guo, E. Leobandung, and S. Y. Chou, A silicon single-electron transistor memory operating at room temperature, *Science* **275**, 649 (1997).
 - ² H. W. C Postma, T. Teepen, Z. Yao, M. Grifoni, and C. Dekker, Carbon nanotube single-electron transistors at room temperature, *Science* **293**, 76 (2001).
 - ³ S. Kubatkin, A. Danilov, M. Hjort, J. Cornil, J. L. Bredas, N. Stuhr-Hansen, P. Hedegard, and T. Bjornholm, Single-electron transistor of a single organic molecule with access to several redox states, *Nature* **425**, 698 (2003).
 - ⁴ P. Michler, A. Imamoglu, M. D. Mason, P. J. Carson, G. F. Strouse, and S. K. Buratto, Quantum correlation among photons from a single quantum dot at room temperature, *Nature* **406**, 968 (2000).
 - ⁵ C. Santori, D. Fattal, J. Vuckovic, G. S. Solomon, and Y. Yamamoto, Indistinguishable photons from a single-photon device, *Nature* **419**, 549 (2002).
 - ⁶ W. H. Chang, W. Y. Chen, H. S. Chang, T. P. Hsieh, J. I. Chyi, and T. M. Hsu, Efficient single-photon sources based on low-density quantum dots in photonic-crystal nanocavities, *Phys. Rev. Lett.* **96**, 117401 (2006).
 - ⁷ S. Gustavsson, M. Studer, R. Leturcq, T. Ihn, K. Ensslin, D. C. Driscoll and A. C. Gossard, Frequency-selective single-photon detection using a double quantum dot, *Phys. Rev. Lett.* **99**, 206804 (2007).
 - ⁸ M. Josefsson, A. Svilans, A. M. Burke, E. A. Hoffmann, S. Fahlvik, C. Thelander, M. Leijnse, H. Linke, A quantum-dot heat engine operating close to the thermodynamic efficiency limits, *Nature Nanotechnology* **13**, 920 (2018).
 - ⁹ C. R. Kagan and C. B. Murry, Charge transport in strongly coupled quantum dot solids, *Nature Nanotechnology* **10**, 1013 (2015).
 - ¹⁰ T. C. Harman, P. J. Taylor, M. P. Walsh, and B. E. LaForge, Quantum dot superlattice thermoelectric materials and devices, *Science* **297**, 2229 (2002).
 - ¹¹ E. Talgorn, Y. Gao, M. Aerts, L. T. Kunneman, J. M. Schins, T. J. Savenije, Marijn A. van Huis, Herre S. J. van der Zant, Arjan J. Houtepen and Laurens D. A. Siebbeles, Unity quantum yield of photogenerated charges and band-like transport in quantum-dot solids, *Nature Nanotechnology* **6**, 733 (2011).
 - ¹² W. I. L. Lawrie, H. G. J. Eenink, N. W. Hendrickx, J. M. Boter, L. Petit, S. V. Amitonov, M. Lodari, B. Wuetz Paquelet, C. Volk, S. G. J. Philips et al, Quantum dot arrays in silicon and germanium, *Appl. Phys. Lett.* **116**, 080501 (2020).
 - ¹³ K. S. Novoselov, A. K. Geim, S. V. Morozov, D. Jiang, Y. Zhang, S. V. Dubonos, I. V. Grigorieva, and A. A. Firsov, Electric field effect in atomically thin carbon films, *Science* **306** 666 (2004).
 - ¹⁴ A. K. Geim, and I. V. Grigorieva, Van der Waals heterostructures, *Nature* **499**, 419 (2013).
 - ¹⁵ K. S. Novoselov, A. Mishchenko, A. Carvalho, and A. H. C. Neto, 2D materials and van der Waals heterostructures,

- Science **353**, aac9439 (2016).
- ¹⁶ S. B. Desai, G. Seol, J. S. Kang, H. Fang, C. Battaglia, R. Kapadia, J. W. Ager, J. Guo, and A. Javey, Strain-Induced Indirect to Direct Bandgap Transition in Multi layer WSe₂, *Nano Lett.* **14**, 4592 (2014).
 - ¹⁷ J. Cai, P. Ruffieux, R. Jaafar, M. Bieri, T. Braun, S. Blankenburg, M. Muoth, A. P. Seitsonen, M. Saleh, X. Feng, K. Mullen, and Roman Fasel, Atomically precise bottom-up fabrication of graphene nanoribbons, *Nature* **466**, 470 (2010).
 - ¹⁸ J. Z. Liu, B. W. Li, Y. Z. Tan, A. Giannakopoulos, C. Sanchez-Sanchez, D. Beljonne, P. Ruffieux, R. Fasel, X. L. Feng, K. Mullen, Toward Cove-Edged Low Band Gap Graphene Nanoribbons, *J. Am. Chem. Soc.* **137**, 6097 (2015).
 - ¹⁹ Y. C. Chen, T. Cao, C. Chen, Z. Pedramraz, D. Haberer, D. G. de Oteyza, F. R. Fischer, S. G. Louie and M. F. Crommie, Molecular bandgap engineering of bottom-up synthesized graphene nanoribbon heterojunctions, *Nature Nanotechnology* **10**, 156 (2015).
 - ²⁰ P. Ruffieux, S. Wang, B. Yang, C. Saez-Saez, J. Liu, T. Dienel, L. Talirz, P. Shinde, C. A. Pignedoli, D. Passerone, T. Dumslaff, X. Feng, K. Mullen, and R. Fasel, On-surface synthesis of graphene nanoribbons with zigzag edge topology, *Nature* **531**, 489 (2016).
 - ²¹ O. Groning, S. Wang, X. Yao, C. A. Pignedoli, G. B. Barin, C. Daniels, A. Cupo, V. Meunier, X. Feng, A. Narita, K. Muellen, P. Ruffieux, and R. Fasel, Engineering of robust topological quantum phases in graphene nanoribbons, *Nature* **560**, 209 (2018).
 - ²² D. J. Rizzo, G. Veber, T. Cao, C. Bronner, T. Chen, F. Zhao, H. Rodriguez, S. G. Louie, M. F. Crommie, and F. R. Fischer, Topological band engineering of graphene nanoribbons, *Nature* **560**, 204 (2018).
 - ²³ L. H. Yan and P. Liljeroth, Engineered electronic states in atomically precise artificial lattices and graphene nanoribbons, *ADVANCES IN PHYSICS: X* **4**, 1651672 (2019).
 - ²⁴ D. J. Rizzo, G. Veber, J. W. Jiang, R. McCurdy, T. Cao, C. Bronner, T. Chen, Steven G. Louie, F. R. Fischer, M. F. Crommie, Inducing metallicity in graphene nanoribbons via zero-mode superlattices, *Science* **369**, 1597 (2020).
 - ²⁵ Q. Sun, Y. Yan, X. L. Yao, K. Mullen, A. Narita, R. Fasel, and P. Ruffieux, Evolution of the Topological Energy Band in Graphene Nanoribbons, *J. Phys. Chem. Lett.* **12**, 8679 (2021).
 - ²⁶ D. J. Rizzo, J. W. Jiang, D. Joshi, G. Veber, C. Bronner, R. A. Durr, P. H. Jacobse, T. Cao, A. Kalayjian, H. Rodriguez, P. Butler, T. Chen, Steven G. Louie, F. R. Fischer, and M. F. Crommie, Rationally Designed Topological Quantum Dots in Bottom-Up Graphene Nanoribbons, *ACS Nano* **15**, 20633 (2021).
 - ²⁷ X. Wang, J. Ma, W. H. Zheng, S. Osella, N. Arisnabarreta, J. Droste, G. Serra, O. Ivasenko, A. Lucotti, D. Beljonne, M. Bonn, X. Y. Liu, M. R. Hansen, M. Tomasini, S. De Feyter, J. Z. Liu, H. I. Wang, X. L. Feng, Cove-Edged Graphene Nanoribbons with Incorporation of Periodic Zigzag-Edge Segments, *J. Am. Chem. Soc.* **144**, 228 (2022).
 - ²⁸ P. A. Almeida and G. B. Martins, Thermoelectric transport properties of armchair graphene nanoribbon heterostructures, *J. Phys: Condens. Matter* **34**, 335302 (2022).
 - ²⁹ M. Topsakal, H. Sevincli, and S. Ciraci, Spin confinement in the superlattices of graphene ribbons, *Appl. Phys. Lett.* **92**, 173118 (2008).
 - ³⁰ H. Sevincli and G. Cuniberti, Enhanced thermoelectric figure of merit in edge-disordered zigzag graphene nanoribbons, *Phys. Rev. B* **81**, 113401 (2010).
 - ³¹ P. Darancet, V. Olevano and D. Mayou, Coherent Electronic Transport through Graphene Constrictions: Sub-wavelength Regime and Optical Analogy, *Phys. Rev. Lett.* **102**, 136803 (2009).
 - ³² G. C. Liang, N. Neophytou, M. S. Lundstrom and D. E. Nikonov, Contact effects in graphene nanoribbon transistors, *Nano. Lett.* **8**, 1819 (2008).
 - ³³ Y. Matsuda, W. Q. Deng, and W. A. Goddard III, Contact Resistance for "End-Contacted" Metal-Graphene and Metal-Nanotube Interfaces from Quantum Mechanics, *J. Phys. Chem. C* **114**, 17845 (2010).
 - ³⁴ P. C. Shen, C. Su, Y. X. Lin, A. S. Chou, C. C. Cheng, J. H. Park, M. H. Chiu, A. Y. Lu, H. L. Tang, M. M. Tavakoli, G. Pitner, X. Ji, Z. Y. Cai, N. N. Mao, J. T. Wang, V. C. Tung, J. Li, J. Bokor, A. Zettl, C. I. Wu, T. Palacios, L. J. Li, and J. Kong, Ultralow contact resistance between semimetal and monolayer semiconductors, *Nature* **593**, 212 (2021).
 - ³⁵ R. S. Chen, G. L. Ding, Y. Zhou and S. T. Han, Fermi-level depinning of 2D transition metal dichalcogenide transistors, *J. Mater. Chem. C* **9**, 11407 (2021).
 - ³⁶ K. Wakabayashi, K. Sasaki, T. Nakanishi and T. Enoki, Electronic states of graphene nanoribbons and analytical solutions, *Sci. Technol. Adv. Mater.* **11**, 054504 (2010).
 - ³⁷ D. M. T. Kuo, Thermoelectric and electron heat rectification properties of quantum dot superlattice nanowire arrays, *AIP Advances* **10**, 045222 (2020).
 - ³⁸ D. M. T. Kuo, Effects of zigzag edge states on the thermoelectric properties of finite graphene nanoribbons, *Jpn. J. Appl. Phys.* **61**, 075001 (2022).
 - ³⁹ D. M. T. Kuo and Y. C. Chang, Contact Effects on Thermoelectric Properties of Textured Graphene Nanoribbons, *Nanomaterials* **12**, 3357 (2022).
 - ⁴⁰ K. Nakada, M. Fujita, G. Dresselhaus and M. S. Dresselhaus, Edge state in graphene ribbons: Nanometer size effect and edge shape dependence, *Phys. Rev. B* **54**, 17954 (1996).
 - ⁴¹ K. Wakabayashi, M. Fujita, H. Ajiki, and M. Sigrist, Electronic and magnetic properties of nanographite ribbons, *Phys. Rev. B* **59**, 8271 (1999).
 - ⁴² T. Gunst, T. Markussen, A. P. Jauho, and M. Brandbyge, Thermoelectric properties of finite graphene antidot lattices, *Phys. Rev. B* **84**, 155449 (2011).
 - ⁴³ P. H. Chang, M. S. Bahrany, N. Nagaosa, and B. K. Nikolic, Giant Thermoelectric Effect in Graphene-Based Topological Insulators with Heavy Adatoms and Nanopores, *Nano Lett.* **14**, 3779 (2014).
 - ⁴⁴ Y. T. Zhang, Q. M. Li, Y. C. Li, Y. Y. Zhang and F. Zhai, Band structures and transport properties of zigzag graphene nanoribbons with antidot array, *J. Phys: Condens. Matter* **22**, 315304 (2010).
 - ⁴⁵ T. Chu, and Z. Chen, Understanding the Electrical Impact of Edge Contacts in Few-Layer Graphene. *ACS Nano* **8**, 3584 (2014).
 - ⁴⁶ C. Gong, S. McDonnell, X. Y. Qin, A. Azcatl, H. Dong, Y. J. Chabal, K. Cho, and R. M. Wallace, Realistic Metal-Graphene contact structures. *ACS Nano* **8**, 642 (2014).
 - ⁴⁷ S. M. Song, T. Y. Kim, O. J. Sul, W. C. Shin, and B. J. Cho, Improvement of graphene-metal contact resistance by introducing edge contacts at graphene under metal, *Appl.*

- Phys. Lett. **104**, 183506 (2014).
- ⁴⁸ Q. Gao, and J. Guo, Role of chemical termination in edge contact to graphene. APL Mater. **2**, 056105 (2014).
 - ⁴⁹ Y. Matsuda, W. Q. Deng, and W. A. Goddard, Contact resistance properties between nanotubes and various metals from quantum mechanics. J. Phys. Chem. C **111**, 11113 (2007).
 - ⁵⁰ J. Massen, W. Ji, and H. Guo, First principles study of electronic transport through a Cu(111)/graphene junction. Appl. Phys. Lett. **97**, 142105 (2010).
 - ⁵¹ S. Barraza-Lopez, M. Vanevic, M. Kindermann, and M. Y. Chou, Effects of Metallic Contacts on Electron Transport through Graphene. Phys. Rev. Lett. **104**, 076807 (2010).
 - ⁵² C. Shen, J. Liu, N. Jiao, C. X. Zhang, H. Xiao, R. Z. Wang and L. Z. Sun. Transport properties of graphene/metal planar junction. Phys. Lett. A **378**, 1321 (2014).
 - ⁵³ Q. Ran, M. Gao, X. Guan, Y. Wang, and Z. Yu, First principles investigation on bonding formation and electronic structure of metalgraphene contacts. Appl. Phys. Lett. **94**, 103511 (2009).
 - ⁵⁴ K. Stokbro, M. Engelund, and A. Blom, Atomic-scale model for the contact resistance of the nickel-graphene interface. Phys. Rev. B **85**, 165442 (2012).
 - ⁵⁵ B. Ma, G. Cheng, Y. W. Wen, R. Chen, K. G. Cho, and B. Shan, Modulation of contact resistance between metal and graphene by controlling the graphene edge, contact area, and points defects: An ab initio study, J. Appl. Phys. **115**, 183708 (2014).
 - ⁵⁶ H. C. Qin, W. C. Lu, and J. Bernholca, Ab initio simulations of metal contacts for graphene-based devices, J. Appl. Phys. **131**, 214301 (2022).
 - ⁵⁷ L. Yang, C. H. Park, Y. W. Son, Marvin L. Cohen, and Steven G. Louie, Quasiparticle Energies and Band Gaps in Graphene Nanoribbons, Phys. Rev. Lett. **99**, 186801 (2007).
 - ⁵⁸ G. Lee and K. Cho, Electronic structures of zigzag graphene nanoribbons with edge hydrogenation and oxidation, Phys. Rev. B **79**, 165440 (2009).
 - ⁵⁹ R. S. Whitney, Most Efficient Quantum Thermoelectric at Finite Power Output, Phys. Rev. Lett. **112**, 130601 (2014).
 - ⁶⁰ H. Zheng, H. J. Liu, X. J. Tan, H. Y. Lv, L. Pan, J. Shi, and X. F. Tang, Enhanced thermoelectric performance of graphene nanoribbons, Appl. Phys. Lett. **100**, 093104 (2012).
 - ⁶¹ Y. Xu, Z. Gan, and S. C. Zhang, Enhanced Thermoelectric Performance and Anomalous Seebeck Effects in Topological Insulators, Phys. Rev. Lett. **112**, 226801 (2014).
 - ⁶² R. Golizadeh-Mojarad and S. Datta, Effect of contact induced states on minimum conductivity in graphene, Phys. Rev. B **79**, 085410 (2009).
 - ⁶³ T. Cusati, G. Fiori, A. Gahoi, V. Passi, M. C. Lemme, A. Fortunelli, and G. Iannaccone, Electrical properties of graphene-metal contacts, Scientific Reports, **7**, 5109 (2017).
 - ⁶⁴ D. M. T. Kuo and Y. C. Chang, Thermoelectric and thermal rectification properties of quantum dot junctions, Phys. Rev. B **81**, 205321 (2010).
 - ⁶⁵ D. M. T. Kuo, S. Y. Shiau, and Y. C. Chang, Theory of spin blockade, charge ratchet effect, and thermoelectrical behavior in serially coupled quantum dot system, Phys. Rev. B **84**, 245303 (2011).
 - ⁶⁶ D. M. T. Kuo, C. C. Chen and Y. C. Chang, Large enhancement in thermoelectric efficiency of quantum dot junctions due to increase of level degeneracy, Phys. Rev. B **95**, 075432 (2017).